RSC Advances

Design of Graphene Oxide-SnO2 Nanocomposite with Superior Catalytic Efficiency for the Synthesis of β-enaminones and β-enaminoesters

Journal:	*RSC Advances*
Manuscript ID:	RA-ART-02-2015-003363.R1
Article Type:	Paper
Date Submitted by the Author:	02-Apr-2015
Complete List of Authors:	Kumar, Aniket; National Institute of Technology, Chemistry Rout, Lipeeka; National Institute of Technology, Chemistry Dhaka, Rajendra; Indian Institute of Technology Delhi, Physics Samal, Saroj; National Institute of Technology, Chemistry Dash, Priyabrat; National Institute of Technology, Rourkela,

Graphene-SnO_2 nanocomposite has been synthesized by solvothermal method, which is more effective and less time-consuming catalyst for the synthesis of β-enaminones and β-enaminoesters.

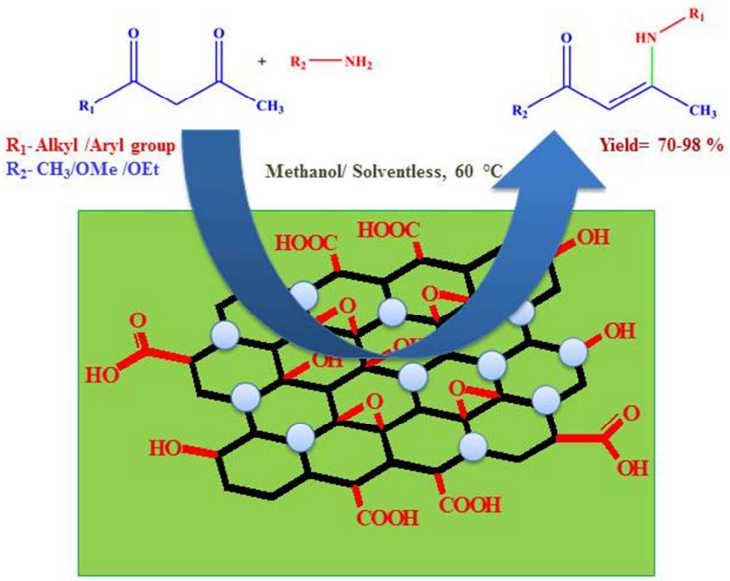

Journal Name

RSCPublishing

ARTICLE

Design of Graphene Oxide-SnO_2 Nanocomposite with Superior Catalytic Efficiency for the Synthesis of *β*-enaminones and *β*-enaminoesters

ββCite this: DOI: 10.1039/xoxxoooooox

Received ooth January 2012,
Accepted ooth January 2012

DOI: 10.1039/xoxxoooooox

www.rsc.org/

Aniket Kumar,[a] Lipeeka Rout,[a] Rajendra S. Dhaka,[b] Saroj L. Samal,[a] and Priyabrat Dash*[a]

[a] Department of Chemistry, National Institute of Technology, Rourkela, Odisha, India, 769008
[b] Department of Physics, Indian Institute of Technology, Delhi, New Delhi, India, 110016

Graphene oxide (GO)-SnO_2-based nanocomposite was synthesized by decorating graphene oxide surface with SnO_2 nanoparticles via a solvothermal process. The nanocomposite was characterized using Fourier transform infrared spectra (FTIR), FT-Raman spectroscopy, X-ray diffraction (XRD), X-ray photoelectron spectroscopy (XPS), Field-emission Scanning electron microscopy (FE-SEM), Energy dispersive X-ray spectroscopy (EDS), Transmission electron microscopy (TEM) and N_2 adsorption-desorption study. The FE-SEM and TEM images demonstrate the uniform distribution of the SnO_2 nanoparticles on the GO surface and high-resolution transmission electron microscopy (HRTEM) confirms an average particle size of 8–12 nm. GO-SnO_2 nanocomposite has been found to be an extremely efficient catalyst for the synthesis of *β*-enaminones and *β*-enaminoester in methanol solvent and also, in solventless condition. The GO-SnO_2 nanocomposites exhibited synergistically more superior catalytic efficiency compared to pure graphene oxide and SnO_2 nanoparticles.The reaction conditions were optimized by changing different parameters such as catalyst, solvent, catalyst loading, and temperature. It has been found that the catalyst gave higher activity under solventless condition than methanol. GO-SnO_2 composite was recycled up to four cycles with minimal loss in activity.

1. Introduction

Fine chemicals are considered as chemicals that are manufactured to high and well-defined standards of purity. These chemicals are a highly multifaceted class of intermediates for the synthesis of heterocyclic and biologically active compounds.[1, 2] β-enaminones have emerged as one of the finest bio-active intermediates in the field of organic chemistry. In particular, the enaminones and enaminonester moiety has attracted much interest, because it is a fundamental and versatile starting material for synthesis of heterocycles,[3] alkaloids,[4, 5],γ-amino alcohol,[6] quinolines,[7] azocompounds[8] and α,β-amino acids.[9, 10] In addition, it serves as a basic synthon for various pharmaceutical drug molecules that control physiological actions, such as anti-bacterial,[11, 12] anticonvulsant,[13] anti-tussive,[14] anti-inflammatory,[15] anti-tumor drugs.[16] The scientific community thus seeks for economic synthesis of such fine chemicals. The conventional synthesis protocols used for *β*-enaminones and *β*-enaminoesters involved condensation of carbonyl compounds with amines catalyzed by metal oxides,[19] chlorides,[17, 18] aurates,[20] SiO_2 and it's composite,[16, 21-23] ionic liquids,[24] and triflates.[25-27] Owing to its high surface to volume ratio and lack of residual energy, metallic nanoparticles have also been a topic of interest for *β*-enaminone synthesis.[28-30] The basic drawbacks which the previous reaction strategies undergo include requirements for particular reaction environment,[25] hygroscopic triflate precursors,[25, 27] use of homogeneous catalyst,[31-33] formation of side products, requirement of extended reaction time,[34, 35] non-reusability of the catalyst,[33] use of expensive reagents,[36, 37] and use of toxic reagents and solvents.[38, 39] Therefore, improved synthesis routes in terms of minimal side-products, product purity and catalyst recovery are highly desirable in fine chemical synthesis.[40] Keeping all this in mind, the development of reusable heterogeneous supported catalyst under non-toxic and solventless condition has become more desirable.[41, 42] In order to meet these requirements, supported metal oxide nanocomposites are found to be preferable materials as solid-state catalysts owing to their nanometric size that contributes to the dramatic increase in their surface area.

Graphene oxide, a two-dimensional sheet of sp^2 hybridized carbon, has received increasing attention as it possesses similar properties to that of graphene, as well as the availability of polar functional groups such as hydroxyl, carboxyl, etc. on its planar surface. Because of its high surface area, thermal stability, mechanical and electrical properties, it can be used as a significant supporting material and has already shown many promising applications.[43] Moreover, the design of GO-based nanocomposites, generated by decorating GO surface with metal oxide nanoparticles, have further extended its applications. These GO-metal oxide nanocomposites have been found as promising materials for fuel cells,[44] sensors,[45] solar cells,[46] lithium batteries,[47] and organic synthesis.[48] In context to catalysis, the presence of various functional groups, larger surface area, and high thermal strength makes GO as a promising material

for catalysis. These oxygenated functional groups can serve as nucleation sites for metal and metal oxide ions to form GO-based nanocomposites. The main advantages of nanocomposite materials, such as high thermal stability, high strength and chemical resistance make them great choice for designing the catalytic system. Though GO based systems has been studied for various catalytic reactions such as coupling reaction,[49, 50] reduction reaction [51] and oxidation reaction. [52, 53] To the best of our knowledge, the use GO-based system for fine chemical syntheses has not been demonstrated so far.

Among various metal oxide nanoparticles, tin oxide (SnO_2) has a wide band gap n-type semiconductor and is found to be suitable material for different applications such as sensors,[54] hydrogenation catalyst,[55] barrier layers for solar cells,[56] optoelectronic devices,[57] liquid crystal displays [58] and as anode material in lithium-based batteries.[59] Moreover, recently, they have found potential application in catalysis.[60, 61-62] Tin oxide has been widely used as a catalyst in chemical reactions, including oxidation and synthesis of vinyl ketone, because of its excellent catalytic properties in the adsorption and dissociation of various molecules.[63] Also, as tin (IV) oxide exhibits redox catalytic properties, these may be modified substantially by the incorporation of other molecules to further upgrade its catalytic efficiency. [63, 64] Additionally, SnO_2 nanostructures could have additional advantages in enhancing the catalytic activities because such structures can potentially not only have high surface area but also helps in more efficient transport for the reactant molecules to get to the active sites. Therefore, combination of GO with SnO_2 can lead to a potential catalytic system for various reactions.

As a part of our own work towards the development of improved catalytic systems, we have considered the use of graphene oxide (GO) as a support for various metal oxide nanoparticles and use them as a catalyst in organic synthesis. In this direction, we were interested in investigating GO-SnO_2 based system as a novel catalyst for fine chemical synthesis. Generally, GO is densely surrounded by polar oxygen-containing functional groups, such as hydroxyl, epoxy, and carboxyl groups, and it was envisaged that these groups would be able to coordinate to the SnO_2 species and prevent them from aggregating and leaching. Moreover, due to its pronounced cations exchange capacity and intercalation ability, GO would be an ideal catalyst support material, and for the intercalation of catalytically active SnO_2 species.[65] Herein, we report for the first time the design of GO-SnO_2 nanocomposite as an efficient catalyst for the synthesis of β-enaminones and enaminoesters. The nanocomposite used was prepared by a simple solvothermal method that is inexpensive and requires a lesser amount of time. The structural and catalytic properties of the GO-SnO_2 nanocomposites were thoroughly investigated by various techniques. The GO-SnO_2 nanocomposite demonstrates remarkable activity with high yield of products for a wide variety of amine and dicarbonyl precursors. All the reaction proceeded in a shorter period of time compared to traditional catalysts. Moreover, the catalyst can be recycled and reused up to four cycles with minimal loss in activity in solventless system.

2. Experimental

2.1 Materials

Graphite powder, $CDCl_3$ and $SnCl_4{\cdot}5H_2O$ were purchased from Sigma-Aldrich. H_2O_2 (30%), isopropanol, ethanol, $NaNO_3$, H_2SO_4 (98%), HCl, $KMnO_4$, and silica gel (100-200 mesh) were purchased from Hi-Media. All chemicals were used as received without further purification. 18 MΩ cm Milli-Q water was used throughout the synthesis.

2.2 Preparation of GO

GO was prepared from natural graphite powder through modified Hummer's method.[66-68] In a typical synthesis, 1 g of graphite was added to 25 ml to conc H_2SO_4 (98% w/w), followed by stirring at room temperature for 24 h. After that 100 mg of $NaNO_3$ was added to the mixture and stirred for 30 min. Subsequently, the mixture was kept below 5 ^{0}C using an ice bath, and 3 g of $KMnO_4$ was slowly added to the mixture and the mixture was stirred for 2 h under ice-water bath. About 250 ml distilled water and 20 ml H_2O_2 (30%) was added to dilute the solution at room temperature. The suspending solution was allowed to precipitate for 12 h and later on, the upper supernatant was collected and centrifuged. Successively, the GO powders were washed with 10% HCl and distilled water three times. The obtained GO was dispersed in distilled water to get a stable brown solution.

2.3 Preparation of GO-SnO_2 nanocomposites

Graphene oxide–SnO_2 nanocomposites were prepared via a solvothermal method. In a typical synthesis, a required amount of 0.02 g of $SnCl_4{\cdot}5H_2O$ and 50 mg of GO were added in 50 ml of isopropanol, followed by sonication for 1 h to obtain a completely dispersed solution. Afterward, 2 ml of deionized water was added dropwise, followed by stirring for another 30 min. After that, the aqueous dispersion was transferred into a 100 ml Teflon-lined, stainless-steel autoclave and heated at 180 ^{o}C for 16 h. The products were then collected by centrifugation and washed several times with water and ethanol in order to remove the chloride ion. The resulting precipitates were dispersed in water for characterizations and further use.

2.4 Characterization

The catalyst was analyzed by X-Ray diffraction study using PHILIPS PW 1830 X-ray diffractometer with CuK_α source. The compositional information of the products was performed using EDX (JEOL JSM-6480 LV). Raman spectra were recorded using a BRUKER RFS 27 spectrometer with 1064 nm wavelength incident laser light. Field emission scanning electron microscopy (FESEM) of the sample was recorded by Nova NanoSEM/FEI. Transmission electron micrographs (TEM) of the sample was recorded using PHILIPS CM 200 equipment using carbon coated copper grids. Nitrogen adsorption/desorption isotherm was obtained at 77 K on a Quantachrome Autosorb 3-B apparatus. The specific surface area and pore size distribution were acquired by emulating BET equation and BJH method, respectively. ^{1}H NMR and ^{13}C NMR spectra were recorded on a Bruker spectrometer at 400 MHz using TMS as an internal standard. FTIR spectra of the product were recorded using a Perkin-Elmer FTIR spectrophotometer using NaCl support. A commercial electron energy analyzer (PHOIBOS 150 from Specs GmbH, Germany) and a non-monochromatic Mg Ka x-ray source ($h\nu$ = 1253.6 eV) have been used to perform XPS measurements with the base pressure of $< 1 \times 10^{-9}$ mbar. Catalytic reactions were monitored by thin layer chromatography on 0.2 mm silica gel F-254 plates. All the reaction products are known compounds and have been identified by comparing their physical and spectral characteristics with the literature reported values.

3. Results and discussion

Structure and morphology characterization

In this work, graphene oxide was synthesized using hummer's methods as discussed in the experimental section. Later on, a solvothermal method was employed for the fabrication of GO-SnO_2 composite using $SnCl_4 \cdot 5H_2O$. The presence of various chemical groups on both GO and GO-SnO_2 was characterized by XRD and FTIR spectroscopy. Fig.1. shows the typical XRD pattern of as prepared GO and GO-SnO_2 nanocomposite. The X-ray diffraction peak of GO show a sharp peak at $2\Theta=10.5^0$ which relates to the (002) reflection of stacked GO sheets. The diffraction peaks (100), (110), (101), (200), (211), (310) and (301) as seen in the XRD profile in Fig.1(b). can be indexed to the rutile phase of SnO_2 (JCPDS no. 41-1445). It is interesting to note that no distinct peaks related to graphene oxide were observed in the powder X-ray diffraction pattern, which could be due to low crystallinity of GO in the GO-SnO_2 composite and sufficient deposition of SnO_2 nanoparticles onto the GO surface. Additionally, it also suggests that SnO_2 nanoparticles possibly acted as a spacer to separate the GO sheets resulting in a decrease of the restacking problems in the composite. By Scherrer equation, the average crystallite size of SnO_2 nanoparticles was found to be around 10 nm from (110) and (101) diffraction peak of GO-SnO_2, which is in a good agreement with the HRTEM findings as discussed in the later part of the discussion.

Further, the nature of chemical groups and the deoxygenating degree of oxygen functional groups in GO and GO-SnO_2 samples were characterized using FT-IR spectroscopy (Fig.2 (a-b)). As depicted in Fig. 2a. FT-IR spectrum of GO revealed the presence of oxygenated functional groups such as structural -OH near 3412 cm^{-1}, C−O−C at 1051 cm^{-1}, and C=O in carboxylic acid moieties at 1726 cm^{-1}. Other characteristic vibrations were the O–H deformation peak at 1405 cm^{-1} and the C–O stretching peak at 1043 cm^{-1}. These results suggest the abundance of hydroxyl groups on the surface of GO. The peak around 1182 cm^{-1} is attributed to C-H bending vibration of the aromatic ring present in GO-SnO_2 nanocomposite.[69, 70] However, in GO-SnO_2 composite, the O−C−O vibration and structural O−H peak disappeared and the intensity of the C−O−C and C=O peaks significantly decreased, suggesting the effective reduction of oxygen-containing functional groups of GO in GO-SnO_2 nanocomposite. Furthermore, the presence of Sn−O−Sn symmetric stretching (668 cm^{-1}) and Sn−O asymmetric stretching (539 cm^{-1}) in GO-SnO_2, as opposed to that of GO, demonstrate the successful incorporation of SnO_2 nanoparticles in GO nanosheets.

The surface composition and chemical states of the individual species in GO-SnO_2 nanocomposite were evaluated by XPS analysis. Fig. 3a. shows the XPS survey scan of GO-SnO_2 in the wide energy range, revealing the presence of carbon, oxygen and tin species without the detection of any other hetero elements. Two symmetrical peaks at 488 eV and 496.5 eV in the Sn 3d spectrum (Fig. 3b) can be attributed to Sn $3d_{5/2}$ and Sn $3d_{3/2}$ binding energy, respectively, which are, in well agreement with the energy splitting reported for bare SnO_2.[71] These values correspond to the 3d binding energy of Sn(IV) ions. The spin-orbit splitting of Sn 3d is observed about 8.5 eV while the area ratio of the two peaks ($3d_{5/2}$ and $3d_{3/2}$) is 1.5. The interaction of SnO_2 with GO in GO-SnO_2 can be confirmed by the presence of an O 1s peak at 533 eV in the XPS spectra (Fig.3a), which corresponds to the oxygen species in the SnO_2. In addition, an increase in the peak-to-peak separation from 8.2 ± 1 eV in bare SnO_2 nanoparticles [72] to 8.5 eV in the GO-SnO_2 composite suggest the binding of SnO_2 with GO nanosheets. For GO, the main peak positioned at around 284.5 eV, is assigned to non-oxygenated ring carbon molecules, while alternate peaks at 286.7, 287.8 and 289.1 eV are assigned to the oxygen- containing groups (C–OH), (C=O), and (O=C–OH), respectively (Fig.3c). The C 1s XPS range of the GO–SnO_2 demonstrates that there is no significant change in intensity of the oxygenated functionalities in comparison to that of GO as shown in Fig. 3d., demonstrating that no effective change in functional group present on GO happened during the nanocomposite synthesis.

The detailed morphology and internal structure of GO-SnO_2 composite were further studied by FE-SEM and TEM as shown in Fig. 4(a-e). The FE-SEM image of GO (Fig. 4a) shows well-established layered structure with sub-micrometre size pores. It is observed that the layered structure of GO was maintained in the composite after decoration with SnO_2 nanoparticles (Fig.4b). Fig. 4c displays the TEM image of GO-SnO_2 composite under a low magnification, where numerous SnO_2 nanoparticles can be seen attached onto the GO surface. It was found that small sized uniform SnO_2 nanoparticles are anchored on GO. No apparent aggregation of SnO_2 nanoparticles on the GO sheet were observed. This type of coverage of SnO_2 nanoparticle on GO surface decreases the restacking of graphene oxide sheets, thereby increase the stability of individual graphene oxide sheets.[73] Additionally, the contour of individual SnO_2 nanoparticles can be seen in Fig. 4d. Fig. 4e. shows the high-resolution TEM image of GO-SnO_2 composite where the lattice fringe of each SnO_2 nanoparticle can be clearly observed. From the size distribution chart, the average size of the SnO_2 nanoparticles was found to be around 8-12 nm (Fig. 4f). This lattice-resolved HRTEM image shows interplanar spacing of 0.33 nm and 0.26 nm, which corresponds to (110) and (101) planes of rutile phases of SnO_2, respectively.[74] The corresponding selected area electron diffraction (SAED) pattern shown in Fig. 4g. have sharp diffraction spots indicating single crystalline nature of SnO_2 nanoparticles in the nanocomposite. The EDS spectrum of the GO-SnO_2 (Fig. 4h) exhibits the presence of C, O, and Sn elements suggesting the formation of GO-SnO_2 nanocomposite via solvothermal process demonstrated in the work.

To obtain further understanding of the structural changes occurs during the chemical processing from GO to GO-SnO_2, Raman spectra were obtained and are shown in Fig. 5. The Raman spectrum of pure graphene oxide displays a D-band at 1310 cm^{-1}, typically assigned to defects and disarranged structures of GO lattice.[75] Another peak at 1603 cm^{-1} was also seen which is assigned to the G-band obtained due to the vibration of sp^2-bonded carbon atoms in the hexagonal lattice. In comparison, the D and G- Raman band of the composite are positioned at a different position like 1290 cm^{-1} and 1593 cm^{-1}, respectively. A careful search on the literatures reveal that when metal nanoparticles are deposited on the surface of GO, the intensity ratio of D and G-band (I_D/I_G) usually increase, suggesting the presence of electronic interaction between the nanoparticles and GO.[76] In our case, the intensity ratio of composite (I_D/I_G=1.19) is found to be larger than that of the pure graphene oxide (I_D/I_G=0.94). Additionally, the peak position of G- band was shifted from 1603 cm^{-1} in GO to 1593 cm^{-1} in GO-SnO_2 composite. These Raman results suggest the presence of electronic interaction between SnO_2 and GO in the composite, thus confirming the successful incorporation of the SnO_2 particles onto the GO surface. Furthermore, these results are consistent with the TEM and XPS results. It is important to note that similar geometrical confinement of metal oxide nanoparticles decorated on graphene nanosheets had been reported in various literatures, to suppress the agglomeration of nanoparticles.[77-79]

From XRD findings, it was found that SnO_2 possibly act as a spacer during the composite synthesis resulting in the decrease of restacking of GO sheets. In reality, this should lead to an increase in the surface area of the composite.[80, 81] To gain insights about this possible impact, N_2 adsorption-desorption isotherm of GO and GO-

SnO_2 composite were carried out and are shown in Fig. 6(a-b). Both the samples exhibit type IV isotherm with an associated H3-type hysteresis loop based on the IUPAC classification.[78] The average pore diameters in GO and GO–SnO_2 composite were found to be 4.4 nm and 5 nm, respectively, whereas, BET surface areas were 100 m^2g^{-1} and 128 m^2g^{-1}, respectively. This higher surface area of GO–SnO_2 suggests the successful decoration of SnO_2 nanoparticles on GO surface. Moreover, this observed increase in the surface area could be one of the factors responsible for the enhanced catalytic activity of the GO–SnO_2 composite discussed later in detail. Additionally, TGA was employed for the estimation of weight percentage of SnO_2 in GO-SnO_2 composite (Fig. 7). A weight loss of ~ 4 wt% was observed before 100 ºC due to the evaporation of moisture content. In comparison, a bigger weight loss happened in the range of 300-500 ºC, corresponding to the decomposition of graphene sheets.[82] From the analysis, the SnO_2 content in the composite was found to be ~70 wt%.

Catalytic activity

At first, condensation of benzylamine with acetylacetone was chosen as a model reaction (scheme. 1). In order to find the best catalyst, the model reaction was carried out using graphite, GO, SnO_2, and GO-SnO_2. Among all, GO-SnO_2 composite was found to be the most efficient catalyst providing an excellent yield of 96 % (Table 1, entry 4). In comparison, the reaction using bulk SnO_2 nanoparticle produced a yield 48% (Table 1, entry 3) of the desired product as compared to graphite (10%) (Table 1, entry 1) and GO (30%) (Table 1, entry 2). Later on, the impact of various reaction parameters such as solvent, catalyst loading, temperature, and time was studied (Table 1, entries 6-23). Appropriately, a blank reaction was performed using 1 mmol proportionate each of commercially available acetylacetone and benzylamine. The reaction did not move ahead satisfactory even after prolonged reaction time and only traces of product was obtained (Table 1, entry 5). The influence of various solvents like methanol, ethanol, acetonitrile, DCM, THF, DMSO, dioxane and hexane on the condensation of the model reaction was then studied (Table 1, entries 6–12). More precisely, it is interesting to note that the yield of product increases with increase in polarity of the solvent. Again polar solvents have very high affinity towards the hydrophilic pores of GO-SnO_2 nanocomposite and the reactions occur with the high catalytic efficiency. [83] Additionally, enhance reactivity can be attributed to the strong hydrogen bond interaction in methanol solvent, which stabilizes the reaction intermidiates and enhances the rate of reaction. [84, 85] The reaction was also carried out under solventless conditions to evolve the influence of the solvent parameter, and product was obtained in good yield with less reaction time (Table 1, entry 13). It was observed that the reaction provided best result when methanol was used as solvent (96 % yield), which was then, employed for further study along with solventless system (98% yield). The activity of catalyst without solvent remains constant after 40 min i.e 98 %. In an effort to demonstrate the catalytic efficiency of GO-SnO_2, various catalyst loadings were then investigated (Table 1, entries 14–17). The yield was found to increase with the increase in catalyst loading in the range of 5 to 15 wt%. Best result with respect to yield was obtained when 10 wt% of SnO_2 nanoparticles was used (Table 1, entries 15,17). No significant increase in yield happened when catalyst loading was increased beyond 10 wt % (Table 1, entry 16). Lastly, effect of different temperatures on the activity for GO-SnO_2 composite for model reaction was studied at varying temperatures ranging from room temperature (r.t.) to reflux condition. It was observed that with the increase in temperature the yield of desired product initially increased (Table 1, entries 18–23). However, at a temperature, i.e., reflux condition, the yield was decreased, reflecting 60 °C as the optimum temperature. Hence, the optimum reaction conditions were catalyst: GO-SnO_2 composite, solvent: methanol and solventless system, catalyst loading of 10 wt %, temp: 60 °C and time: 75 min.

In order to check the generality of the above reaction protocol, the optimized conditions were then applied for the enamination of diketones with various amines, providing excellent yields of the products as shown in Table 2 (entries 1-33). All the reactions were completed within 20-210 min at 60 ^{0}C temperature to give the desired products in excellent yields (75-98%) without forming any side products.The ^{1}H and ^{13}C NMR data of products are provided in supplementary information file. It was exciting to know that the condensation products of *β*-enaminones and *β*-enaminonesters were obtained in excellent yield under solventless conditions in lesser time with respect to the systems containing methanol solvent. While a few past methodologies for similar reaction conditions showed negative results and extremely poor yield [18, 86], the system (GO-SnO_2) developed here was found to be more promising for the *β*-enaminones and *β*-enaminonesters synthesis. Acetyl acetone reacts with aniline to give a good yield of product of around 92% in methanol solvent and 96% in solventless system (Table 2, entry 5). Similarly excellent yield of the condensation product was obtained in case of aliphatic and acyclic amine such as methylamine, ethylamine, propylamine, butylamine and morpholine (Table 2, entries 1-4, 7), when GO-SnO_2 nanocomposite was used as a catalyst. It was found that the reaction with aliphatic amines proceeds easily in a short period of time as compared to aromatic amine. From our observations, it could be justified that the lower nucleophilicity of aromatic amines as compared to the aliphatic amines could be the reason for higher yield obtained in case of aliphatic amines. Moreover, the presence of electron releasing and withdrawing group is found to be a factor in governing the yield of product. For example, an aromatic amine-containing an electron donating substituents such as a methyl group gave good yield (Table 2, entry 10). Further, the yield of condensation product obtained for o-nitroaniline and p-nitroaniline (Table 2, entries 8-9) precursor, was slightly lower which can be attributed to electron withdrawing nature of nitro group which supresses the yield of the product. So, the presence of electron withdrawing group is also one of the factors which govern the yield of product.

The addition of amines to other dicarbonyl compound like methyl acetoacetate and ethyl acetoacetate was found to give an excellent yield of desired products with same type of aliphatic, acyclic and aromatic amine under optimized conditions (Table 2, entries 11-33) .To confirm the role of the catalyst, a blank reaction was carried out under similar reaction conditions with model reaction in absence of catalyst, but, no progress was found even after stirring for a long reaction time. It clearly establishes the role of catalyst GO-SnO_2 composite for activation of the carbonyl group.

The proposed mechanism for the condensation reaction is shown in scheme 2. Typically, the condensation of dicarbonyl compounds with aliphatic and aromatic amines proceeds through an addition-elimination reaction. In GO-SnO_2, the GO surface acts as an acidic site that helps the keto form of the dicarbonyl compound (1A) to get converted into more favorable and active enol form (1B). The lone pair of nitrogen of the amine then adds to the enolic carbonic centre to generate a tetrahedron intermediate after passing through a four-centered transition state (I,II).[87] In the same time, Tin oxide has a Lewis acid site Sn^{4+} and Lewis basic sites O^{2-}.[88] The lewis acid site, Sn (IV) of SnO_2 molecule that anchored onto the GO surface co-ordinate with the other carbonyl oxygen of the diketone, thereby stabilizing the transition state further. Finally, the tetrahedron

intermediate undergoes an elimination of the water molecule to generate the imine moiety. The imine intermediate (IV) after tautomerization forms the enaminones as the final product. It can be concluded that the Sn (IV) of SnO_2 nanoparticle help in activation and stabilization of subsrate molecules during enaminones and enaminoester synthesis.

General procedure for the synthesis of *β*-enaminones in solvent media

In a 50 ml round bottom flask, GO-SnO_2 nanocomposite (0.02 g) as a catalyst was taken in methanol (5 ml) and stirred at room temperature for 10 minutes. Then, a mixture of amine (1 mmol) and *β*-dicarbonyl compound (1 mmol) were added to it and stirred at 60 ºC under nitrogen atmosphere. The advancement of reaction was monitored by TLC. On completion of the reaction as indicated by TLC examination, the catalyst was filtered off. Evaporation of the solvent followed by column chromatography on silica-gel column gave the pure enaminones as the final products.

General procedure for the synthesis of *β*-enaminones under solventless condition

In a 50 ml round bottom flask, mixture of amine (1 mmol), *β*-dicarbonyl compound (1 mmol), and GO-SnO_2 nanocomposite (0.02 g) as catalyst was taken and stirred at 50 ºC under nitrogen atmosphere. The advancement of reaction was monitored by TLC. On completion of the reaction as indicated by TLC examination, the mixture was diluted with EtOAc (5 mL) and filtered. The catalyst was recovered by filtration from residue. The filtrate was concentrated and product was purified by column chromatography on silica gel using EtOAc/hexane as eluent. Recovered catalyst was washed with water followed by acetone (3x10 mL) and dried at 150 ºC for 1 h, before reusing.

The concentrated product was extracted three times with ethyl acetate (20 ml) and the combined layer were dried over anhydrous Na_2SO_4. The solvent was removed in vacuum. Subsequently, pure *β*-enaminone as a product was obtained by doing column chromatography using silica gel and EtOAc/hexane. The structures of all the products were unambiguously established on the basis of their spectral analysis. All the product were identified by comparing with available literatures.

Reproducibility of catalyst

As discussed earlier, reusability of the heterogeneous catalyst plays an important role in order demonstrate it as economical. Because of this, a series of reaction cycles were run in order to investigate the efficiency of our catalytic system. Recyclability of the catalyst was studied for the model reaction comprising of acetylacetone and benzyl amine in methanol and solventless system. After each catalytic cycle, the catalyst was recovered by centrifugation method, thoroughly washed with polar organic solvents (ethylacetate) to remove all the organic substances and finally dried for 10 h before performing the next cycle with an equal amount of substrate loading. When methanol was used, the recyclability of the catalyst was found to be undesirable and the activity was almost lost. This slow decrease of the catalytic efficiency may be credited to the fact that after each catalytic run we continuously lose some amount of catalyst during the catalyst recovery process and hence the effective loading of the catalyst keeps on decreasing from one catalytic cycle to the next. [89]In methanol medium, the yield of the product decreased significantly to 48% after 4th run (Fig. 8). However, in solventless condition, GO-SnO_2 could be recovered and reused several times. It was observed that there is no significant loss of activity after four cycles, and the yield of the model reaction was 91% after 4th run (Fig. 8).

Comparison with other reported systems

Later on, to check the efficiency of our catalyst we have compared the activity of our catalyst with other reported catalysts. Table 3 shows the comparison of reported catalyst with our catalyst for the synthesis of *β*-enaminones and *β*-enaminoesters under the same conditions. From Table 3, it can be seen that our catalyst exhibited higher yields in lesser time compared to the other reported system such as Cu/AlO(OH) [87], Ag/Fe_3O_4@meso-SiO_2 , B_2O_3/Al_2O_3[90], Ag nanoparticle [28] and PPA-SiO_2 [91]. These results confirmed that our GO-SnO_2 catalyst is more effective and less time consuming for synthesis of *β*-enaminones and *β*-enaminoesters.

4. Conclusions

In summary, we have successfully synthesized GO-SnO_2 nanocomposite catalyst via a solvothermal method. The synthesized catalyst was then characterized using FTIR, XRD, FESEM, TEM, BET, XPS, FT-Raman and EDX techniques. The particle size of nanocomposite was found to be around 8-12 nm. For the first time, GO-SnO_2 nanocomposite shows remarkably higher catalytic activity for the synthesis of fine chemicals such as *β*-enaminones and β-enaminoesters. The nanocomposite catalyst offers several advantages, including high yield, short reaction time, simple work up procedure, ease of separation and easy recyclability of the catalyst. The catalyst was reused up to four runs in solventless system without any significant loss in activity.

Acknowledgements
The authors are thankful to Department of Science & Technology (DST), Govt. of India, for funding and the Sophisticated Analytical Instrument Facility, IIT Madras for providing FT-RAMAN facility. XPS facility at IIT Delhi is partially funded by FIST grant of DST, India.

References

1. G. J. Reddy, D. Latha, C. Thirupathaiah and K. S. Rao, *Tetrahedron Lett.* , 2005, **46**, 301 – 302.
2. G. Negri, C. Kascheres and A. J. Kascheres, *J. Heterocycl. Chem.* , 2004, **41**, 461 – 491.
3. K. V. Tarasenko, O. V. Manoylenko, V. P. Kukhar, G.-V. Röschenthaler and I. I. Gerus, *Tetrahedron Lett.*, 2010, **51**, 4623-4626.
4. G. Li, K. Watson, R. W. Buckheit and Y. Zhang, *Org. Lett.*, 2007, **9**, 2043-2046.
5. B. A. D. Neto, A. A. M. Lapis, A. B. Bernd and D. Russowsky, *Tetrahedron Lett.*, 2009, **65**, 2484-2496.
6. I. Chaaban, J. V. Greenhill and P. Akhtar, *J. Chem. Soc., Perkin Trans. 1* 1979, **6**, 1593-1596.
7. L. J. O. Figueiredo and C. Kascheres, *J. Org. Chem.*, 1997, **62**, 1164-1167.
8. T. Mahmud, R. Rehman, A. Gulzar, A. Khalid, J. Anwar, U. Shafique, Z. Waheed and M. Salman, *Arab. J. Chem.*, 2010, **3**, 219-224.
9. C. Cimarelli and G. Palmieri, *J. Org. Chem.*, 1996, **61**, 5557–5563.
10. D. Potin, F. Dumas and J. D. Angelo, *J. Am. Chem. Soc.*, 1990, **112**, 3483–3486.

11. N. N. Salama, K. R. Scott and N. D. Eddington, *Biopharm. Drug. Dispos.*, 2004, **25**, 227-236.
12. I. O. Edafiogho, O. A. Phillips, E. E. Udo, S. Samuel and B. Rethish, *Eur. J. Med. Chem.*, 2009, **44**, 967-975.
13. A. Z. El-Hashim, I. O. Edafiogho, S. M. Jaffal, M. H. Yousif, C. I. Ezeamuzie and S. B. Kombian, *Life Sci.* , 2011, **89**, 378-387.
14. A. El-Hashim, S. Yousefi, I. Edafiogho, R. Raghupathy, M. Yousif and H.-U. Simon, *Eur. J. Pharmacol.*, 2010, **632**, 73-78.
15. D. L. Boger, T. Ishizaki, R. J. Wysocki, S. A. Munk, P. A. Kitos and O. Suntornwal, *J. Am. Chem. Soc.*, 1989, **111**, 6461-6463.
16. H. Eshghi, S. M. Seyedi, E. Safaei, M. Vakili, A. Farhadipour and M. Bayat-Mokhtari, *J. Mol. Catal. A: Chem.*, 2012, **363–364**, 430-436.
17. J. Lin and L.-F. Zhang, *Monatsh. Chem.*, 2007, **138**, 77-81.
18. M. M. Khodaei, A. R. Khosropour and M. Kookhazadeh, *Synlett*, 2004, **11**, 1980-1984.
19. Z. H. Zhang, T. S. Li and J. J. Li, *Catal. Commun.*, 2007, **8**, 1615-1620.
20. A. Arcadi, G. Bianchi, S. D. Giuseppe and F. Marinelli, *Green Chem.*, 2003, **5**, 64-67.
21. B. Das, K. Venkateswarlu, A. Majhi, M. R. Reddy and K. N. Reddy, *J. Mol. Catal. A :Chem.*, 2006, **246**, 276–281.
22. A. R. Gholap, N. S. Chakor, T. Daniel, R.J.Lahoti and K.V.Srinivasan, *J. Mol. Catal. A :Chem.*, 2006, **245**, 37–46.
23. H. Seki and G. I. Georg, *J. Am. Chem. Soc.*, 2010, **10**, 15512–15513.
24. J.Kang, F.Liang, S.G.Sun, Q. Liu and X. H. Bi, *Org. Lett.*, 2006, **8**, 2547–2550.
25. F. Epifano, S. Genovese and M. Curini, *Tetrahedron Lett*, 2007, **48**, 2717-2720.
26. M. M. Khodaei, A. R. Khosropour and M. Kookhazadeh, *Can. J. Chem.*, 2005, 209-212.
27. J. S. Yadav, V. N. Kumar, R. S. Rao, A. D. Priyadarshini, P. P. Rao, B. V. S. Reddy and K. Nagaiah, *J. Mol. Catal. A: Chem.*, 2006, **256**, 234-237.
28. K. D. Bhatte, P. J. Tambade, K. P. Dhake and B. M. Bhanage, *Catal. Commun.* , 2010, **11**, 1233-1237
29. J. Sun, Z. Dong, P. Li, F. Zhang, S. Wei, Z. Shi and R. Li, *Mater. Chem. Phys.*, 2013, **140**, 1-6.
30. M. Kidwai, S. Bhardwaj, N. K. Mishra, V. Bansal, A. Kumar and S. Mozumdar, *Catal. Commun.*, 2009, **10**, 1514-1517.
31. B. Giuseppe, B. Marcella, L. Manuela, M. Enrico, M. Paolo and S. Letizia, *Synlett*, 2004, **10**, 239–242.
32. Z. H. Zhang, L. Yin and Y. M. Wang, *Adv. Synth. Catal.*, 2006, **348**, 184–190.
33. Z. Zhan-Hui and H. Jin-Yong, *J. Braz. Chem. Soc.*, 2006, **17**, 1447–1451.
34. M. E. F. Braibante, H. S. Braibante, L. Missio and A. Andricopulo, *Synthesis*, 1994, 898–900.
35. Y. Gao, Q. Zhang and J. Xu, *Synth. Commun.*, 2004, **34**, 909–916.
36. M. A. P. Martins, C. P. Frizzo, D. N. Moreira, F. A. Rosa, M. R. B. Marzari, N. Zanatta and H. G. Bonacorso, *Catal. Commun.*, 2008, **9**, 1375–1378.
37. C. P. C. Marin, D. G. Henderson and R.W. Soeder, *Synth. Commun.*, 1997, **27**, 4275–4283.
38. A. R. Katritzky, Y. Fang, A. Donkor and J. Xu, *Synthesis*, 2000, 2029–2032.
39. E. Haak, *Synlett*, 2006, **12**, 1847–1848.
40. P. T. Anastas and R. H. Crabtree, in *Handbook of Green Chemistry Green Catalysis*, 2009, vol. Wiley-VCH.
41. D. Choudhary, S. Paul, R. Gupta and J. H. Clark, *Green. Chem.*, 2006, **8**, 479-482.
42. H. Sharghi, A. Khoshnood and R. Khalifeh, *Iran. J. Sci. Technol.*, 2012, 25-31.
43. Y. Nishina, J. Miyata, R. Kawaib and K. Gotohb, *RSC Adv.*, 2012, **2**, 9380–9382.
44. G. G. kumar, Z. Awan, K. S. Nahm and J. S. Xavier, *Biosens. Bioelectron.*, 2014, **53**, 528–534.
45. X. Wang, Q. Wang, Q. Wang, F. Gao, F. Gao, Y. Yang and H. Guo, *ACS Appl. Mater. Interfaces*, 2014, **6**, 11573−11580.
46. R. Bajpai, S. Roy, N. Koratkar and D. S. Misra, *Carbon*, 2013, **56**, 56 – 63.
47. L. Dong, M. Li, L.Dong, M. Zhao, J. Feng, Y. Han, J.Deng, X. Li, D. Li and X.Sun, *Int. J. Hydrogen Energy*, 2014, **39**, 16116–16122.
48. R. Nie, J. Shi, S. Xia, L. Shen, P. Chen, Z. Hou and F. S. Xiao, *J. Mater. Chem.*, 2012, **22**, 18115–18118.
49. N. Zhang, H. Qiu, Y. Liu, W. Wang, Y. Li, X. Wang and J. Gao, *J. Mater. Chem.*, 2011, **21**, 11080-11083.
50. A. R. Siamaki, A. E. R. S. Khder, V. Abdelsayed, M. S. El-Shall and B. F. Gupton, *J. Catal.*, 2011, **279**, 1-11.
51. K.-C. Hsu and D.-H. Chen, *Nanoscale Res Lett.*, 2014, **9**, 484-494.
52. X. Chen, G. Wu, J. Chen, X. Chen, Z. Xie and X. Wang, *J. Am. Chem. Soc. Rev*, 2011, **133**, 3693-3695.
53. S. Guo, S. Dong and E. Wang, *ACS Nano*, 2009, **4**, 547-555.
54. F. Xu, M. Deng, G. Li, S. Chen and L.Wang, *Electrochim. Acta.* , 2013, **88**, 59-65.
55. R. Adnan, N. A. Razana, I. A. Rahman and M. A. Farrukh, *J. Chin. Chem. Soc.*, 2010, **57**, 222-229.
56. S. Chappel and A. Zaban, *Sol. Energy Mater. Sol. Cells*, 2002, **71**, 141-152.
57. T. W. Kim, D. U. Lee, D. C. Choo, J. H. Kim, H. J. Kim, J. H. Jeong, M. Jung, J. H. Bahang, H. L. Park, Y. S. Yoon and J. Y. Kim, *J. Phys. Chem. Solids*, 2002, **63**, 881.
58. H. Liu, V. Avrutin, N. Izyumskaya, Ü. Özgür and H. Morkoç, *Superlattices Microstruct.*, 2010, **48**, 458–484.
59. M. S. Niasari, N. Mir and F. Davar, *Inorg. Chim. Acta*, 2010, **363**, 1719-1726.
60. Q. Zhao, Z.Zhang, T. Dong and Y. Xie, *J. Phys. Chem. B*, 2006, **110**, 15152-15156.
61. H. Sharghi, S. Ebrahimpourmoghaddam, R. Memarzadeh and S. Javadpour, *J. Iran. Chem. Soc.* , 2012, **10**, 141-149.
62. K. J. Klanbunde, *Nanoscale Materials in Chemistry*, Wiley, New York, 2001.
63. N. L. V. Carreno, H. V. Fajardo, A. P. Maciel, A. Valentini, F. M. Pontes, L. F. D. Probst, E. R. Leite and E. Longo, *J. Mol. Catal. A: Chem.*, 2004, **207** 91-96.
64. G. C. Bond, L. R. Molloy and M. J. Fuller, *J. Chem. Soc. Chem. Commun.*, 1975, **19**, 796–797.
65. J. Biana, M. Xiaoa, S. J. Wanga, Y. X. Lub and Y. Z. Menga, *Catal. Commun.* , 2009, **10**, 1529–1533.
66. S. J. Park, J. H. An, R. D. Piner, I. Jung, D. X. Y. A. Velamakanni, S. B. T. Nguyen and R. S. Ruoff, *Chem. Mater.*, 2008, **20**, 6592–6594.
67. K. N. Kudin, B. Ozbas, H. C. Schniepp, R. K. Prudhomme, I. A. Aksay and B. Car, *Nano Lett.*, 2008, **8**, 36–41.
68. Y. Xu, K. Sheng, C. Li and G. Shi, *ACS Nano*, 2010, **4**, 4324–4330.
69. S. Min and G. Lu, *J. Phys. Chem. C*, 2011, **115**, 13938–13945.
70. L. Wang, Y. Ye, X. Lu, Z. Wen, Z. Li, H. Hou and Y. Song, *Sci. Rep.*, 2013, **3**, 3568.
71. G. Wang, B. Wang, X. Wang, J. Park, S. Dou, H. Ahnb and K. Kim, *J. Mater. Chem.* , 2009, **19**, 8378–8384.
72. F.Li, J. Song, H. Yang, S. Gan, Q. Zhang, D. Han, A. Ivaska and L. Niu, *Nanotechnology*, 2009, **20**, 455602.
73. H. Seema, K. C. Kemp, V. Chandra and K. S. Kim, *Nanotechnology*, 2012, **23**.
74. S. Zhuang, X. Xu, B. Feng, J. Hu, Y. Pang and G. Zhou, *ACS. Appl. Mater. Interfaces*, 2014, **6**, 613–621.
75. Q. Guo and X. Qin, *ECS. Solid State Lett.*, 2013, M41-M43.
76. S. Li, W. Xie, S. Wang, X. Jiang, S. Peng and D. He, *J. Mater. Chem. A*, 2014, **2**, 17139-17145.
77. S. Yang, W. Yue, J. Zhu, Y. Ren and X. Yang, *Adv. Funct. Mater.*, 2013, **23**, 3570–3576.
78. X. Liu, J. Cui, J. Sun and X. Zhang, *RSC Adv.*, 2014, **4**, 22601-22605.
79. Y.-X. Wang, Y.-G. Lim, M.-S. Park, S.-L. Chou, J. H. Kim, H.-K. Liu, S.-X. Dou and Y.-J. Kim, *J. Mater. Chem. A*, 2014, **2**, 529-534.

80. H. Song, L. Zhang, C. He, Y. Qu, Y. Tian and T. Lv, *J. Mater. Chem.*, 2011, **21**, 5972-5977.
81. X. S. Zhou, L. J. Wan and Y. G. Guo, *Adv. Mater*, 2013, **25**, 2152.
82. S. Li, W. Xie, S. Wang, X. Jiang, S. Peng and D. He, *J. Mater. Chem. A*, 2014, **2**, 17139-17145.
83. S. Ray, A. Bhaumik, A. Dutta and C. Mukhopadhyay, *Catal. Sci. Technol.*, 2013, **3**, 1267--1277
84. N. Ahmed and Z. N. Siddiqui, *J. Mol. Catal. A: Chem.*, 2014, **394**, 232–243.
85. S. Park, J. An, I. Jung, R. D. Piner, S. J. An, X. Li, A. Velamakanni and R. S. Ruoff, *Nano Lett.*, 2009, **9**, 1593-1597.
86. M. M. Khodaei, A. R. Khosropour and M. Kookhazadeh, *Russ. J. Org. Chem.*, 2005, **41**, 1445.
87. S. G. Babu, B. Thomas, A. Nijamudheen, A. Datta and R. Karvembu, *Catal. Sci. Technol.*, 2012, **2**, 1872.
88. M. Batzill and U. Diebold, *Prog. Surf. Sci.*, 2005, **79**, 47–154.
89. Z. N. Siddiqui, N. Ahmed, F. Farooq and K. Khan, *Tetrahedron Lett.*, 2013, **54**, 3599-3604.
90. J. X. Chen, C. F. Zhang, W. X.Gao, H.L.Jin, J. C. Ding and H. Y. Wu, *J. Braz. Chem. Soc.*, 2010, **21**, 1552-1556.
91. M. Nisar, I. Ali, M. R. Shah, M. Qayum, M. Z.-U.-Haq, U. Rashid and M. S. Islam, *Molecules*, 2013, **18**, 15182-15192.

Figure Captions

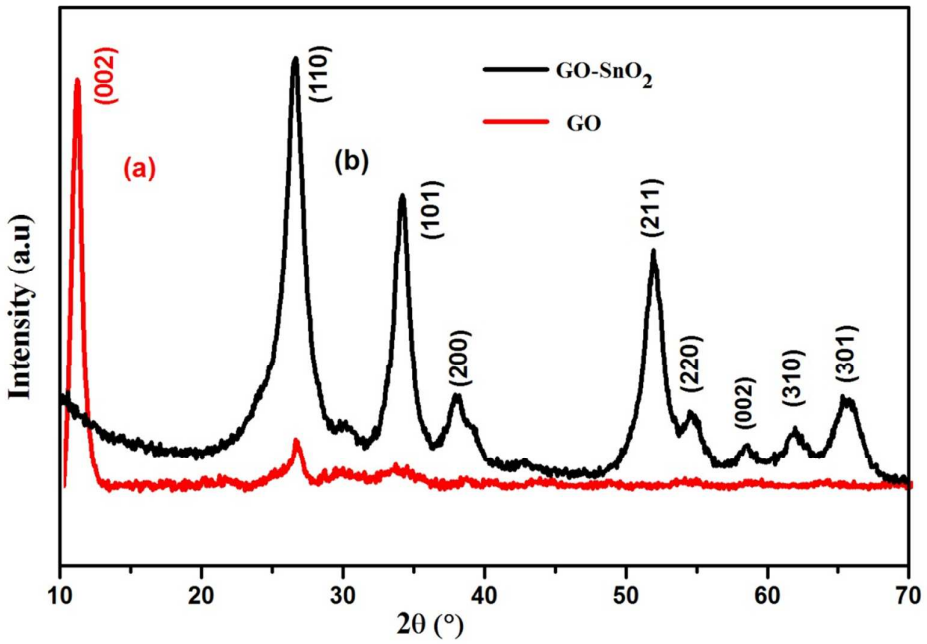

Fig.1. XRD pattern of GO and GO-SnO_2 nanocomposite.

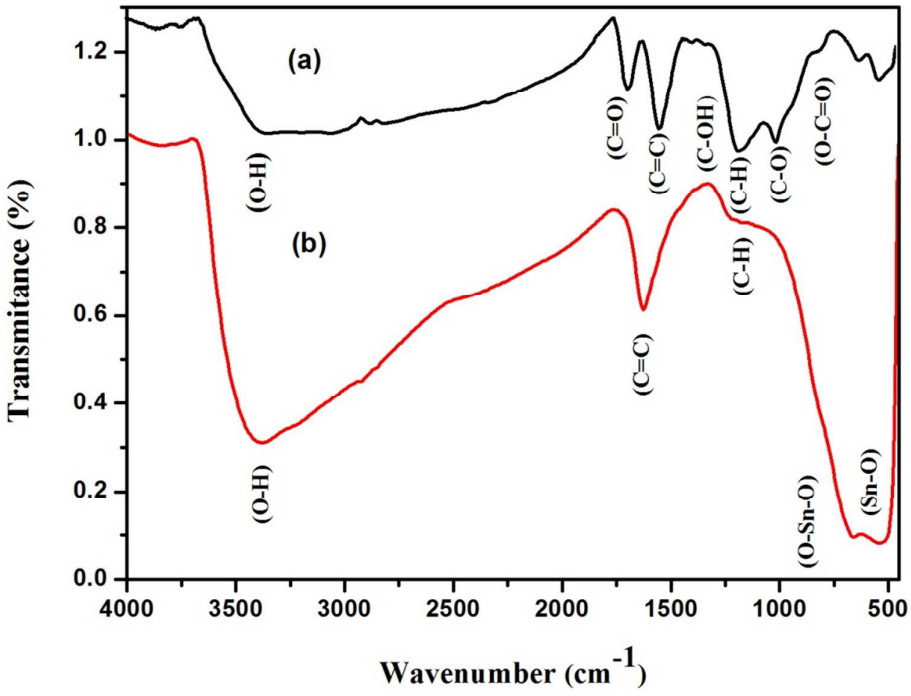

Fig.2. FTIR spectra of (a) GO and (b) GO-SnO_2 nanocomposite .

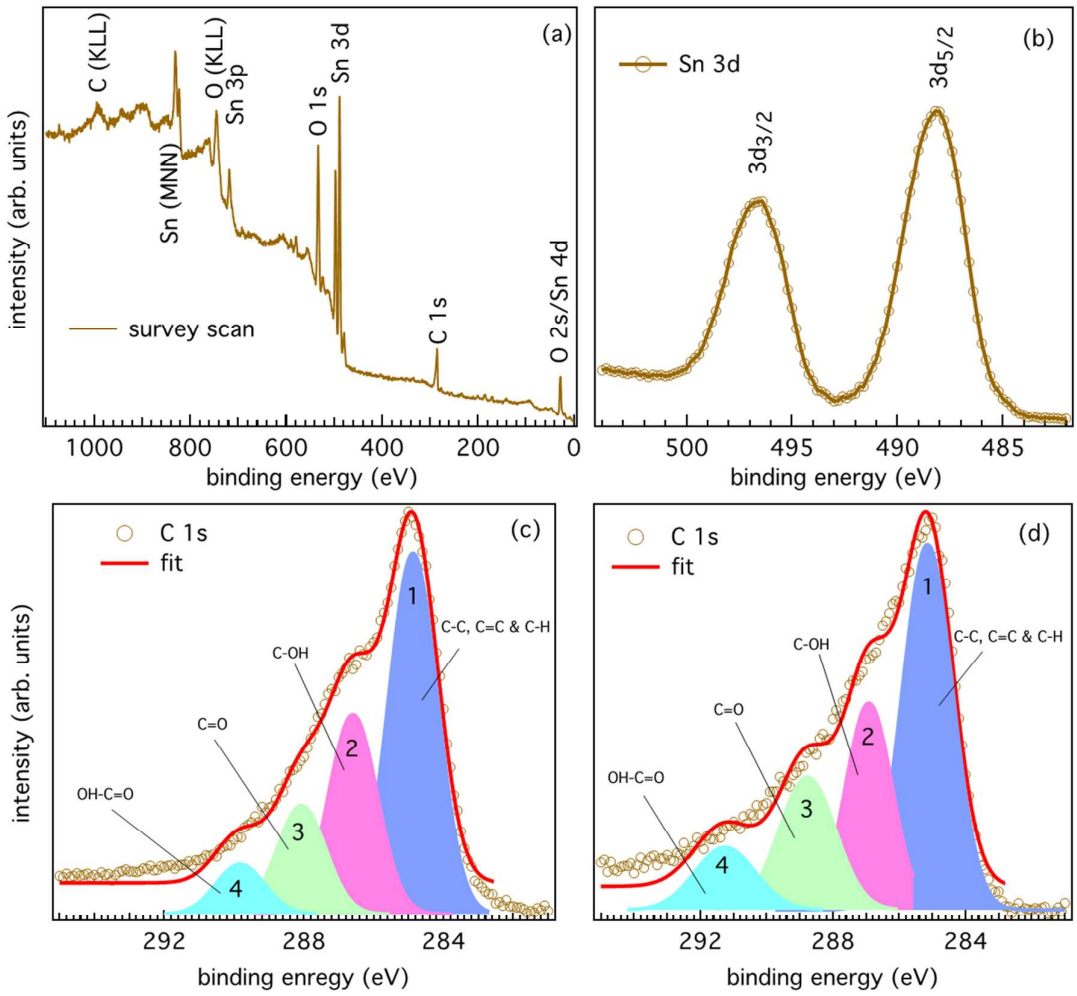

Fig.3. (a) XPS survey spectra of GO-SnO_2 nanocomposite, (b) Sn 3d core level XPS spectra of GO–SnO_2 nanocomposite, (c) C 1s XPS spectra of GO and (d) C 1s XPS spectra GO–SnO_2 nanocomposite.

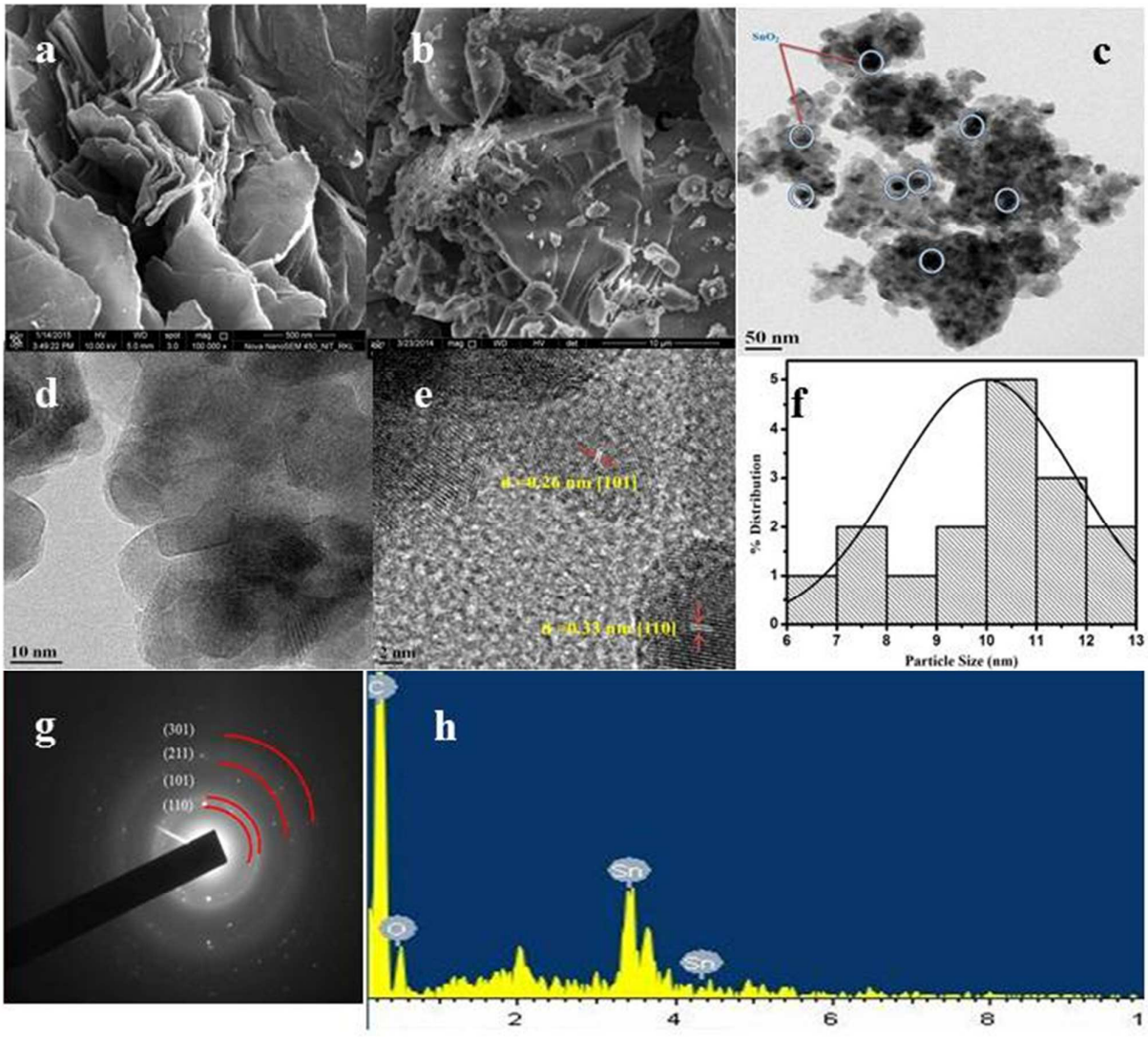

Fig.4. FESEM image of (a) GO, (b) GO-SnO_2 nanocomposite, (c) TEM image of GO-SnO_2 nanocomposite, (d-e) HRTEM image of GO-SnO_2 nanocomposite, (f) size distribution curve of GO-SnO_2 nanocomposite , (g) SAED pattern of GO-SnO_2 nanocomposite and (h) EDX spectra of GO-SnO_2 nanocomposite.

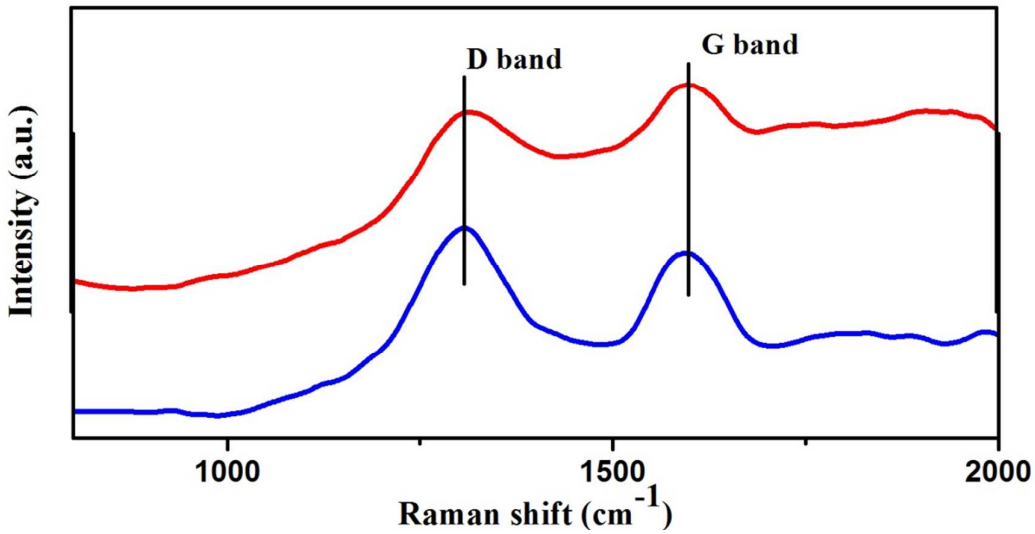

Fig.5. FT-Raman spectra of GO and GO-SnO_2 nanocomposite.

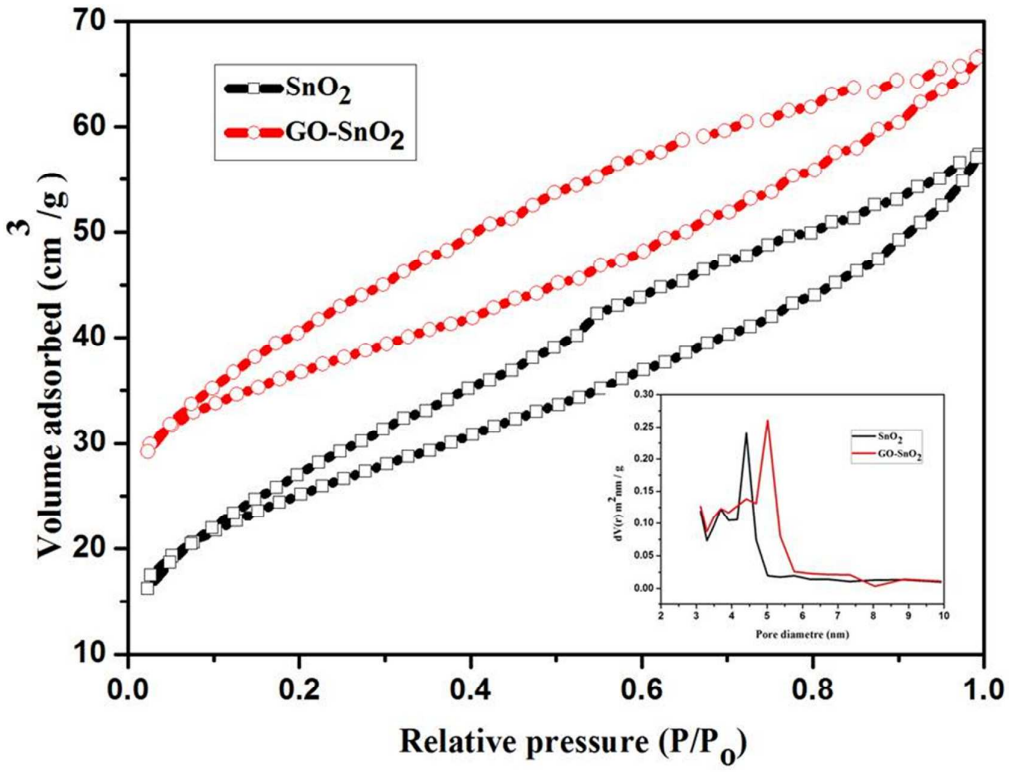

Fig.6. N_2 adsorption-desorption isotherm of SnO_2 and GO-SnO_2 Nanocomposite.

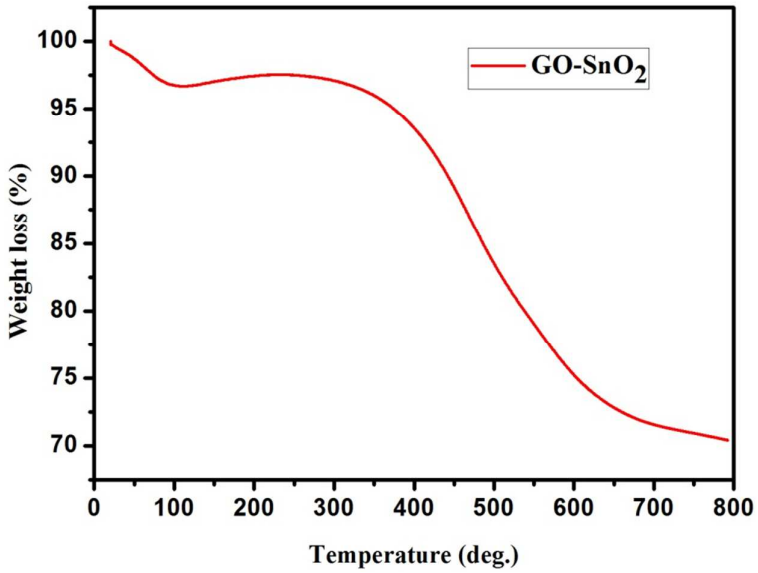

Fig.7. TGA of GO-SnO_2 nanocomposite.

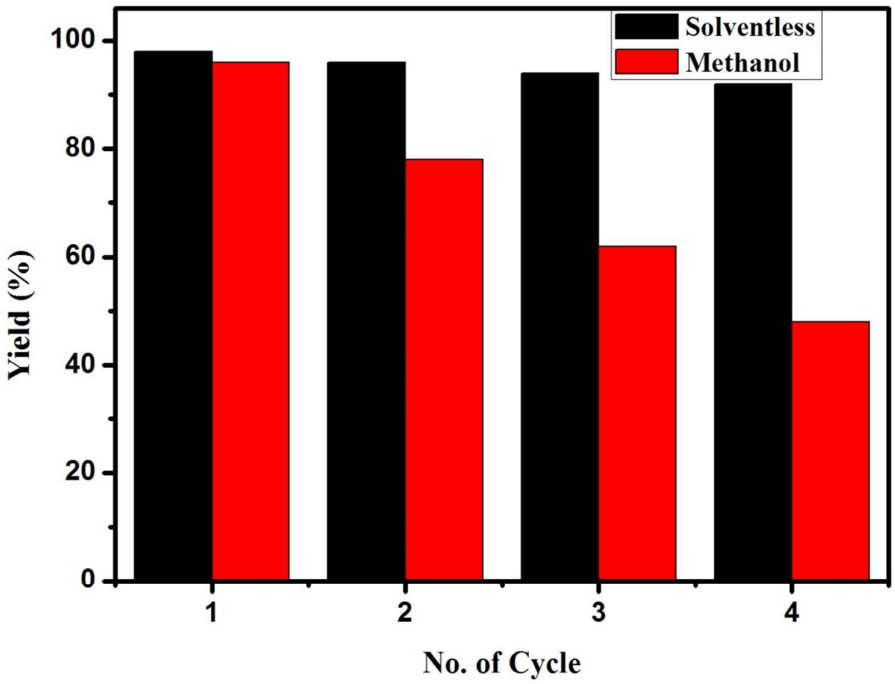

Fig.8. Recyclablity chart for GO-SnO_2 nanocomposite.

Scheme. 1. A model reaction involving condensation of benzyl amine and acetyl acetone.

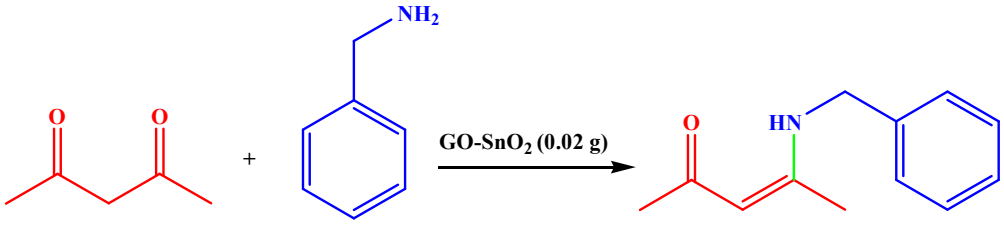

Scheme. 2. Possible mechanistic pathway for the formation of *β*-enaminones.

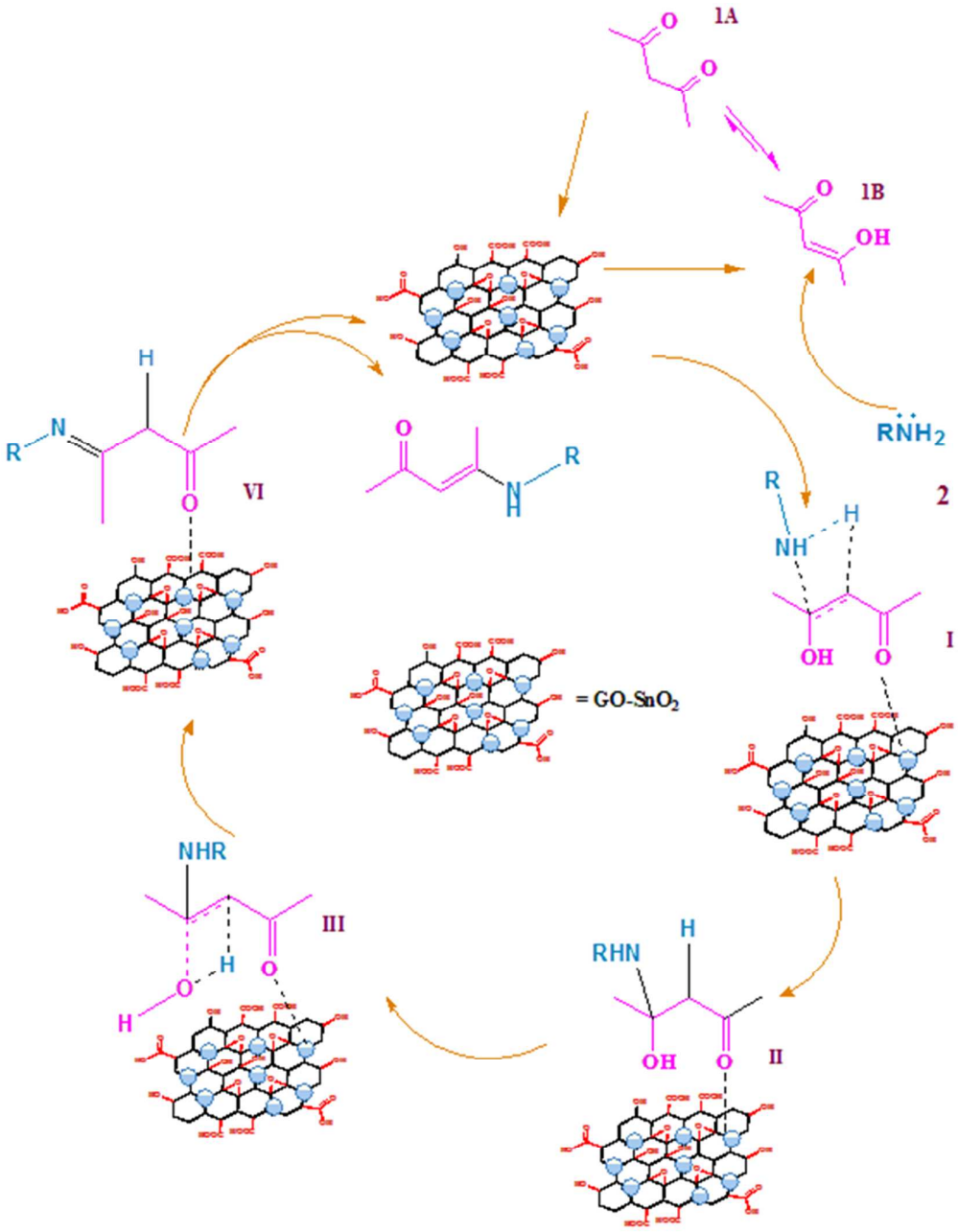

Table.1. Study of reaction parameters on model reaction of benzylamine and acetyacetone.[a]

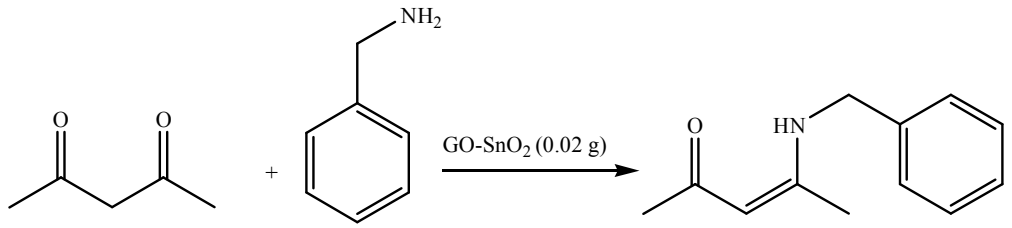

Entry	Solvent	Catalyst	Catalyst loading	Temp (^{0}C)	Yield [b] (%)
Effect of catalyst					
1.	Methanol	Graphite	20 mg	60	10
2.	Methanol	GO	20 mg	60	30
3.	Methanol	SnO_2	10 wt % SnO_2	60	48
4.	Methanol	GO-SnO_2	10 wt % GO/SnO_2	60	96
5.	Methanol	None	---	60	Traces
Effect of Solvent					
6.	Ethanol	GO-SnO_2	10 wt %	60	84
7.	DCM	GO-SnO_2	10 wt %	60	80
8.	Acetonitrile	GO-SnO_2	10 wt %	60	86
9.	THF	GO-SnO_2	10 wt %	60	80
10.	DMSO	GO-SnO_2	10 wt %	60	68
11.	Dioxane	GO-SnO_2	10 wt %	60	82
12.	Hexane	GO-SnO_2	10 wt %	60	20
13.	Solvent less	GO-SnO_2	10 wt %	60	98
Effect of Catalyst loading					
14.	Methanol	GO-SnO_2	5 wt % GO/SnO_2	60	86
15.	Methanol	GO-SnO_2	10 wt % GO/SnO_2	60	96
16.	Methanol	GO-SnO_2	15 wt % GO/SnO_2	60	88
17.	Solventless	GO-SnO_2	10 wt % GO/SnO_2	60	98
Effect of Temperature					
18.	Methanol	GO-SnO_2	10 wt % GO/SnO_2	r.t	48
19.	Methanol	GO-SnO_2	10 wt % GO/SnO_2	45	78
20.	Methanol	GO-SnO_2	10 wt % GO/SnO_2	reflux	82
21.	solventless	GO-SnO_2	10 wt % GO/SnO_2	r.t	54
22.	solventless	GO-SnO_2	10 wt % GO/SnO_2	45	80
23.	solventless	GO-SnO_2	10 wt % GO/SnO_2	reflux	85

[a]Reaction conditions: acetyl acetone (1 mmol), benzaldehyde (1 mmol), Solvent (5 ml), Solventless system and time (75 min).
[b]Isolated Yield.

Table. 2. GO-SnO_2 nanocomposite catalyzed synthesis of a library of β-enaminones and enaminonesters.

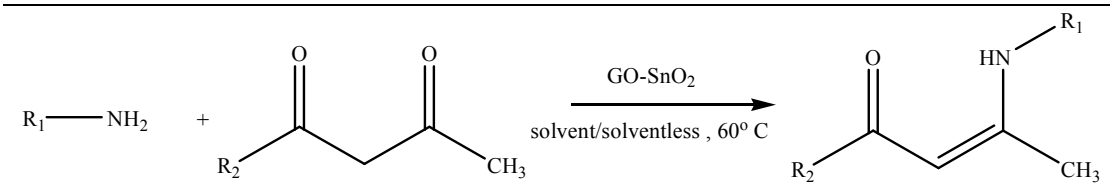

Entry	R_1	R_2	Time(min)/Yield[a](%)	
			Methanol	Solventless
1	CH_3	Me	60/94	40/98
2	C_2H_5	Me	90/90	60/96
3	C_3H_7	Me	60/96	30/98
4	C_4H_9	Me	75/98	40/98
5	Ph	Me	90/92	70/96
6	Ph-CH_2	Me	75/96	40/98
7	C_4H_9NO	Me	120/82	90/86
8	o-$C_6H_6N_2O_2$	Me	110/80	75/80
9	p-$C_6H_6N_2O_2$	Me	100/86	90/89
10	C_8H_{11}	Me	180/72	150/74
11	C_7H_9	Me	100/90	80/92
12	CH_3	OMe	45/92	30/96
13	C_2H_5	OMe	60/88	40/92
14	C_3H_7	OMe	50/94	20/96
15	C_4H_9	OMe	75/88	30/90
16	Ph	OMe	80/92	45/94
17	Ph-CH_2	OMe	60/92	40/96
18	C_4H_9NO	OMe	140/82	100/88
19	o-$C_6H_6N_2O_2$	OMe	190/70	150/76
20	p-$C_6H_6N_2O_2$	OMe	100/92	90/96
21	C_8H_{11}	OMe	220/70	180/76
22	C_7H_9	OMe	100/94	80/96
23	CH_3	OEt	35/96	20/98
24	C_2H_5	OEt	50/94	30/94
25	C_3H_7	OEt	45/92	30/94
26	C_4H_9	OEt	60/90	20/96
27	Ph	OEt	75/94	25/94
28	Ph-CH_2	OEt	75/96	30/94
29	C_4H_9NO	OEt	180/80	120/84
30	o-$C_6H_6N_2O_2$	OEt	210/71	180/74
31	p-$C_6H_6N_2O_2$	OEt	90/92	82/96
32	C_8H_{11}	OEt	200/71	160/96
33	C_7H_9	OEt	90/96	75/98

[a] Reaction condition: amine (1 mmol), 1,3-dicarbonyl compound (1 mmol),GO-SnO_2 nanocomposite (10 wt%), temperature (60 °C), solvent and solventless system.
[b] Isolated Yield

Table. 3. Catalytic performance of different composite material for β-enaminones and enaminonesters

Entry	Catalyst	Solvent	T (^{0}C)	T(min)	Yield(%)	Ref
1	Ag/Fe_3O_4@meso-SiO_2	Methanol	60	60	90	78
2	B_2O_3/Al_2O_3	Ethanol	Room temperature	120	87	29
3	Cu/AlO(OH)	Solventless	27	105	94	79
4	Graphene Oxide-SnO_2	Solventless	60	40	98	This work
5	Graphene Oxide-SnO_2	methanol	60	75	96	This work
6	Silver nanoparticles	methanol	60	120	90	28
7	PPA-SiO_2	methanol	Reflux temperature	130	70	89